Role of chemical pressure on the electronic and magnetic properties of the spin- $\frac{1}{2}$ kagome mineral averievite

Dibyendu Dey * and Antia S. Botana † Department of Physics, Arizona State University, Tempe, Arizona 85287, USA

(Received 17 April 2020; revised 23 July 2020; accepted 24 August 2020; published 8 September 2020)

We investigate the electronic and magnetic properties of the kagome mineral averievite (CsCl)Cu₅V₂O₁₀ and its phosphate analog (CsCl)Cu₅P₂O₁₀ using first-principles calculations. The crystal structure of these compounds features Cu²⁺ kagome layers sandwiched between Cu²⁺-P⁵⁺/Cu²⁺-V⁵⁺ honeycomb planes, with pyrochlore slabs made of corner-sharing Cu tetrahedra being formed. The induced chemical pressure effect upon substitution of V by P causes significant changes in the structure and magnetic properties. Even though the in-plane antiferromagnetic (AFM) coupling J_1 within the kagome layer is similar in the two materials, the interplane AFM coupling J₂ between kagome and honeycomb layers is five times larger in the P variant, increasing the degree of magnetic frustration in the constituting Cu tetrahedra.

DOI: 10.1103/PhysRevB.102.125106

I. INTRODUCTION

Quantum spin liquids (QSLs) represent a novel state of matter in which the constituent spins are highly correlated but still fluctuate so strongly that they prevent long-range magnetic order down to zero temperature [1-5]. These characteristics make them distinct phases of matter, able to display unique exotic behavior such as new types of topological order [6,7], excitations with fractional quantum numbers [8], or certain forms of superconductivity [9,10].

Typically, QSLs are realized in lattices that act to frustrate the appearance of magnetism [3,5]. In two dimensions, the prototypical example is the kagome lattice with spin- $\frac{1}{2}$ ions, which gets realized in a variety of minerals. Herbertsmithite (a copper hydroxychloride mineral with a $Cu^{2+} d^9$ kagome lattice) has been intensively studied in this context [8,11– 15]. This material does not show any signature of long-range magnetic order close to 0 K [8,11], and neutron scattering experiments exhibit a spinon continuum, an indication of fractionalized excitations [8]. However, a major issue concerning herbertsmithite is its intrinsic disorder [16–18] and the fact that doping, which is desirable to give rise to superconductivity, is difficult to achieve [19]. For these reasons, since the discovery of herbertsmithite, other candidate materials have been intensively searched for [20–23].

(CsCl)Cu₅V₂O₁₀ (V-averievite) [24], a fumarolic oxide mineral containing a spin- $\frac{1}{2}$ kagome lattice, has been synthesized and studied in the context of QSL physics [22]. The crystal structure of V-averievite contains Cu²⁺ (spin- $\frac{1}{2}$) kagome layers in which the oxygen environment of the Cu ions is square planar. Each of these kagome planes is sandwiched between two honeycomb layers formed by Cu²⁺ (with a trigonal bipyramidal environment) and V^{5+} (with a tetrahedral environment), as shown in Figs. 1(a)-1(d). The Cu layers form a pyrochlore slab comprising corner-sharing tetrahedra. This tetrahedral geometry introduces magnetic frustration, as interactions within the Cu₄ units are antiferromagnetic (AFM), as shown in Fig. 1(e). Susceptibility data show an AFM phase transition takes place at $T_N = 24 \,\mathrm{K}$ in V-averievite [22]. In a recent experiment [25], Winiarski et al. successfully synthesized (CsCl)Cu₅P₂O₁₀ (P-averievite), the phosphate analog of V-averievite. Substitution of V by P gives rise to differences in structural and magnetic behavior likely due to chemical pressure: the ionic radius of P⁵⁺ in tetrahedral coordination is two times smaller than that of V⁵⁺. Magnetization measurements reveal strong geometric frustration with the susceptibility of P-averievite showing an AFM or spin-glass-like transition at a lower temperature of 3.8 K [25].

In order to understand the change in magnetic response upon chemical pressure in averievite, we use first-principles calculations to obtain a microscopic magnetic model of V and P variants. Our results reveal important differences between the two materials, in particular, the interlayer coupling between Cu kagome and Cu honeycomb atoms is five times larger in the P variant, increasing the degree of magnetic frustration within Cu tetrahedra that constitute a given pyrochlore slab.

II. COMPUTATIONAL DETAILS

Density functional theory (DFT)-based [26,27] calculations have been performed by using a plane-wave basis set and projector augmented-wave potentials [28,29], as implemented in the Vienna Ab initio Simulation Package (VASP) [30,31]. The wave functions were expanded in the plane-wave basis with a kinetic energy cutoff of 500 eV, and the reciprocal space integration was carried out with a Γ centered k mesh of $8 \times 8 \times 6$. For the exchange-correlation functional, the Perdew-Burke-Ernzerhof [32] version of the generalized gradient approximation (GGA) has been used for nonmagnetic

^{*}ddey3@asu.edu

[†]antia.botana@asu.edu

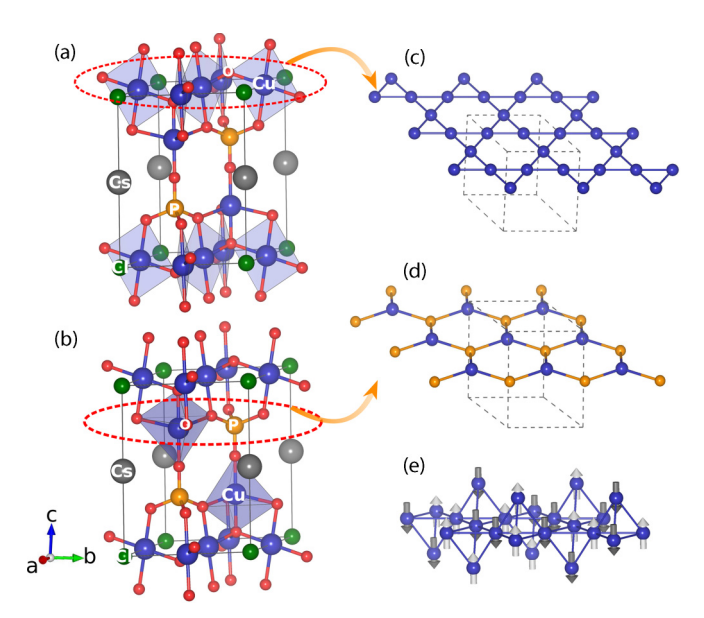


FIG. 1. Crystal structure of P-averievite (V-averievite is isostructural) exhibiting (a) square-planar and (b) trigonal bipyramidal environments for the kagome and honeycomb Cu atoms, respectively. (c) Cu kagome layers are sandwiched between (d) two Cu-P honeycomb layers. Each of these trilayer blocks is separated along the c axis by CsO_2 layers. (e) Cu atoms of adjacent honeycomb and kagome layers form a pyrochlore slab composed of corner-sharing Cu tetrahedra. The corresponding AFM configuration within the Cu tetrahedra is shown. Cs atoms are shown in gray, Cu atoms are in blue, O atoms are in red, P atoms are in golden yellow, and Cl atoms are in green.

calculations. For undoped V- and P-averievite, experimental structural parameters as obtained from synchrotron x-ray diffraction data [22,25] have been used in our calculations. For Zn-doped P-averievite, a full structural relaxation was performed within GGA in the nonmagnetic state until the resulting forces became significantly small (0.01 eV/Å). In order to construct different magnetic configurations, a 2 × 2 × 1 supercell containing 4 f.u. has been used for both undoped and doped compounds. In spin-polarized calculations, strong correlation effects for the Cu 3d electrons have been incorporated within GGA + U using the Dudarev approach [33]. We have used an effective on-site Coulomb repulsion [34], $U_{eff} = U - J = 5 \text{ eV}$, which is reasonable for this type of Cu material [22]. Hopping integrals have been obtained from maximally localized Wannier functions (MLWFs), constructed using WANNIER90 [35].

III. RESULTS AND DISCUSSION

A. Structural and electronic properties

P-averievite crystallizes in a trigonal $P\overline{3}m1$ space group at room temperature, and below 12 K the system undergoes a transition to a monoclinic phase [25]. A similar effect has been reported in V-averievite [22]. Since the structural details of the low-temperature phase are not available, we considered the $P\overline{3}m1$ structure in our calculations for both materials. The crystal structure of P-averievite and its constituent kagome and honeycomb planes, as well as the environments for each

TABLE I. Nearest-neighbor Cu-Cu distances in the kagome plane and Cu-O distances for P-averievite and V-averievite from experimental structural data [22,25]. Cu_k and O_k (Cu_h and O_h) indicate Cu and O atoms in the kagome (honeycomb) planes, respectively. All distances are in angstroms.

	$(CsCl)Cu_5P_2O_{10}\\$	$(CsCl)Cu_5V_2O_{10}$
$\overline{\text{Cu}_k\text{-Cu}_k}$	3.09	3.18
Cu_k - O_k	1.87	1.88
Cu_k - O_h	1.98	2.03
Cu_h - O_h	2.15	2.10
Cu_h - O_k	1.83	1.85

Cu (square planar in the kagome planes, trigonal bipyramidal in the honeycomb ones), are shown in Figs. 1(a)-1(d). The tetrahedra formed by Cu atoms of adjacent honeycomb and kagome layers and the corresponding pyrochlore slab can be seen in Fig. 1(e). Bond lengths for P- and V-averievite from experimental structural data are summarized in Table I. The phosphate material exhibits a lower volume and shorter Cu-Cu and Cu-O bonds due to the smaller size of P: in tetrahedral coordination the ionic radii of P^{5+} and V^{5+} are 0.17 and 0.36 Å, respectively. The Cu_k - O_k - Cu_k and Cu_k - O_k - Cu_h bond angles are $\sim 100^\circ$ in both materials, the latter being 4° larger in P-averievite (106° vs 102°).

We now analyze the effects of P substitution on the nonmagnetic electronic structure of averievite. Figure 2 shows the nonmagnetic GGA band structures, as well as the orbitaland atom-resolved density of states (DOS) for both P- (top panels) and V-averievite (bottom panels). A metallic state is obtained with five Cu bands in the vicinity of the Fermi level E_F in both materials [Figs. 2(a) and 2(e)], in agreement with a Cu²⁺ d^9 configuration. These correspond to $3d_{r^2-v^2}$ kagome Cu bands and $2d_{z^2}$ honeycomb Cu bands, as reflected in the orbital-resolved DOS. This is a consequence of the fact that for the kagome Cu (with square-planar coordination), the $d_{x^2-y^2}$ orbital lies the highest in energy. In contrast, for the honeycomb Cu (with trigonal-bipyramidal coordination and short Cu-O apical bonds along the c axis), the d_{z^2} orbital is the highest in energy. Interestingly, among the five Cu bands, two are separated from the other three bands in P-averievite, unlike in V-averievite. The total DOS plots [Figs. 2(d) and 2(h)] show the large degree of hybridization between O 2p and Cu 3d states in both systems. An important difference is that the valence bandwidth in P-averievite is ~8.5 eV, increased by 1.5 eV with respect to its V counterpart (\sim 7 eV) due to the induced chemical pressure effect upon V by P substitution. In addition, the unoccupied V d states in V-averievite lie approximately 2 eV above the Fermi level [consistent with a V^{5+} d^0 configuration; Fig. 2(h)], whereas the unoccupied P p states appear 7 eV above E_F [Fig. 2(d)].

To further analyze the degree of pd hybridization, hopping integrals $|t_{pd}|$ between O p states and Cu d states have been calculated using MLWFs. To construct a basis of MLWFs we employ a wide energy window that includes the full Cu d manifold, O p, Cl p, and Cs p states. The agreement between the band structure obtained from Wannier function interpolation and that derived from the DFT calculation is excellent (see Appendix A, Fig. 6). The spatial spreads of the

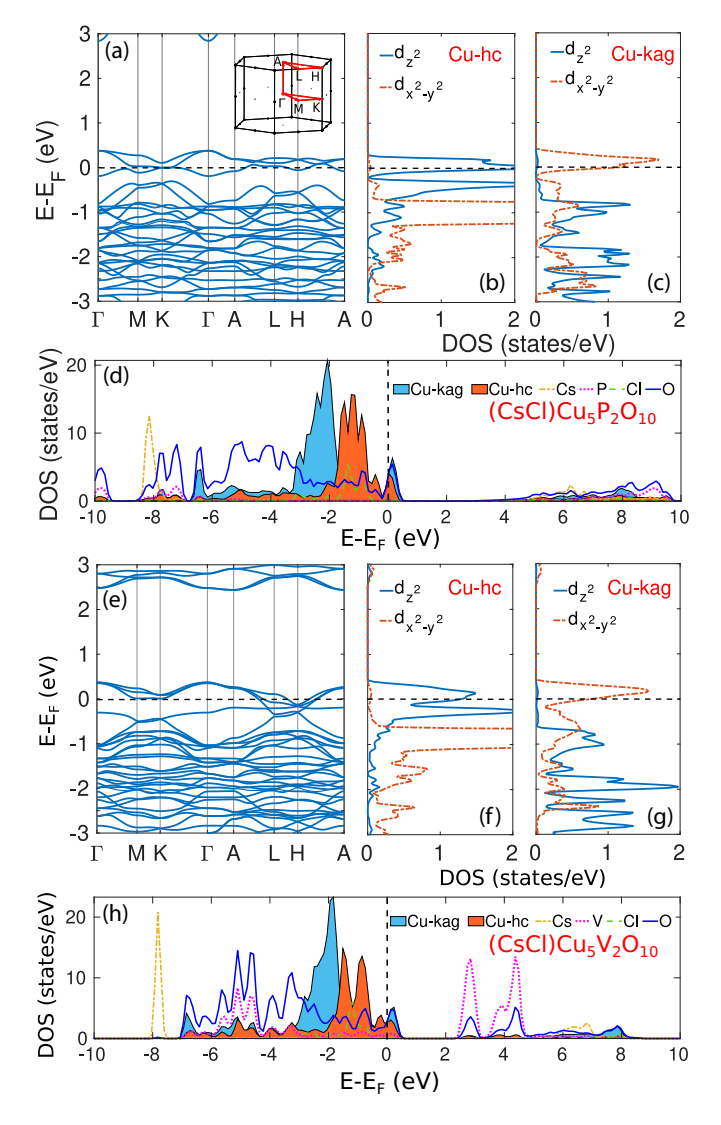


FIG. 2. Nonmagnetic electronic structure of (a)–(d) P-averievite and (e)–(h) V-averievite within GGA. (a) and (e) Band structure, Cu $d_{x^2-y^2}$ and d_{z^2} DOS for (b) and (f) honeycomb and(c) and (g) kagome Cu atoms, and (d) and (h) atom-projected DOS. The band structures are shown along the high-symmetry points $\Gamma = (0,0,0)$, M = (1/2,0,0), K = (1/3,1/3,0), A = (0,0,1/2), L = (1/2,0,1/2), and H = (1/3,1/3,1/2) of the Brillouin zone [shown in the inset in (a)].

Wannier functions are small (\sim 1 Å²). The derived dominant $|t_{pd}|$ integrals are listed in Table II. Overall, the $|t_{pd}|$ hoppings increase in the P system due to the induced chemical pressure effect upon volume reduction, in agreement with the above-described increase in bandwidth in the P material. Only $|t_{pd}|$ between $Cu_k \ d_{x^2-y^2}$ and $O_k \ p_{x,y}$ is unaffected (0.55 eV), whereas the hopping integrals between $Cu_h \ d_{z^2}$ and $O_k \ p_{x,y}$ as well as between $Cu_k \ d_{x^2-y^2}$ and $O_h \ p_{x,y}$ increase significantly in P-averievite (0.97 vs 0.83 eV and 1.15 vs 1.04 eV).

B. Magnetic properties

GGA+U calculations in different magnetic configurations were performed in a $2\times2\times1$ supercell containing 20 inequivalent Cu sites. The magnetic ground state for V-

TABLE II. Leading hopping integrals $|t_{pd}|$ for P- and V-averievite calculated from Wannier functions. $Cu_k(O_k)$ and $Cu_h(O_h)$ represent the copper (oxygen) atoms in the kagome and honeycomb layers, respectively.

$ t_{pd} $ (eV)	(CsCl)Cu ₅ P ₂ O ₁₀	(CsCl)Cu ₅ V ₂ O ₁₀
$\overline{\operatorname{Cu}_k d_{x^2-y^2} - \operatorname{O}_k p_{x,y}}$	0.55	0.55
$\operatorname{Cu}_k d_{x^2-y^2}$ - $\operatorname{O}_h p_{x,y}$	1.15	1.04
$\operatorname{Cu}_h d_{z^2} - \operatorname{O}_k p_{x,y}$	0.97	0.83
$\operatorname{Cu}_h d_{z^2}$ - $\operatorname{O}_h p_{x,y}$	0.40	0.37

and P-averievite is depicted in Fig. 3. This configuration corresponds to AFM nearest-neighbor (NN) coupling in the kagome planes and between the kagome and honeycomb coppers, which gives rise to an AFM configuration on each Cu tetrahedron. Within GGA + U, both compounds exhibit an insulating ground state in this magnetic configuration. The corresponding DOS and band structure are shown in Fig. 4. In P-averievite, the band gap is \sim 0.9 eV, smaller than that for V-averievite, ~ 1.3 eV. Right below the Fermi level, the O p and Cu d character described in the nonmagnetic calculations is kept, but there is also a large contribution of Cl p states to the DOS. This is due to the orientation of the CuO₄ units in the kagome planes, with the Cu d_{z^2} orbitals pointing towards the Cl ion, giving rise to a high degree of hybridization. The unoccupied honeycomb and kagome Cu d states are separated in energy in the phosphate compound, whereas they overlap in the vanadium material. The magnetic moment of Cu atoms in both systems is $0.7\mu_B$, consistent with a d^9 configuration (S=1/2). No sizable moments are developed on other atoms.

The exchange-coupling constants for P- and V-averievite can be obtained by mapping the GGA + U energy differences for different magnetic configurations (see Appendix B for details) to a spin- $\frac{1}{2}$ Heisenberg Hamiltonian of the form

$$H = \sum_{i < j} J_{ij} S_i \cdot S_j. \tag{1}$$

The leading terms are the two nearest-neighbor AFM couplings mentioned above: J_1 between Cu ions in the kagome plane and J_2 between kagome and honeycomb Cu ions (see Fig. 3). Further exchange terms are significantly weaker. Specifically, we find $J_1 = 235$ K and $J_2 = 284$ K for Paverievite, whereas for V-averievite we obtain $J_1 = 228$ K and $J_2 = 52$ K. Notably, J_2 is five times larger in P-averievite. The increase in J_2 in the phosphate material is consistent with the

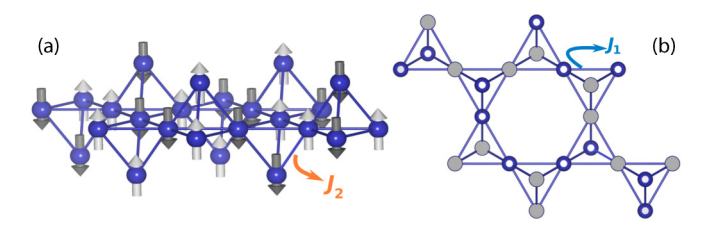


FIG. 3. (a) Magnetic ground state for P- and V-averievite. The two dominant AFM exchange interactions between (b) kagome Cu (J_1) and (a) kagome-to-honeycomb Cu atoms (J_2) are shown.

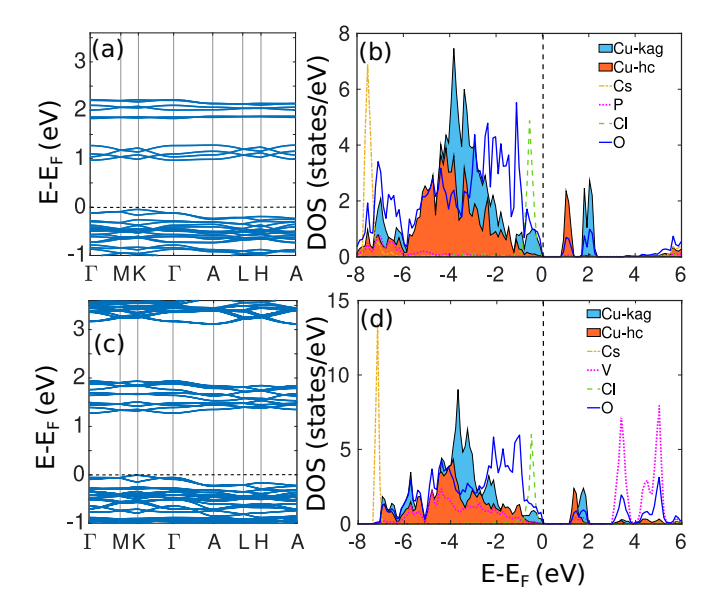


FIG. 4. (a) and (c) GGA + U band structure and (b) and (d) atom-projected density of states of P-averievite (top) and V-averievite (bottom) in the AFM ground state shown in Fig. 3.

above-described hopping integrals and with the increase in the Cu_k - O_k - Cu_h bond angle with respect to its V analog.

In a pyrochlore lattice (or slab) formed by magnetic ions, there is a high degree of frustration when the nearest-neighbor interactions are AFM. This is effectively the situation in Pand V-averievite, in which we find two AFM interactions within a given Cu tetrahedron (J_1 and J_2). In this situation, the more comparable these two AFM interactions are, the larger the degree of magnetic frustration is [36,37]. This is effectively what seems to happen in P-averievite, for which we find comparable J_1 and J_2 and for which the experimentally determined frustration index is larger than that of its V counterpart ($f_{V-\text{averievite}} = \Theta_{CW}/T_t \sim 8$ [22], $f_{P-\text{averievite}} \sim$ 13 [25], where Θ_{CW} is the Curie-Weiss temperature and T_t is the temperature of the magnetic transition). We note that spin-glass-like transitions at low temperature have been reported in other pyrochlore slab materials with strong AFM interactions (i.e., SrCrGaO compounds) [36–38]. This seems to be consistent with experimental data in P-averievite that show a lowering of the magnetic transition temperature with respect to the V-based material and point to the possibility of a spin-glass transition in the P system [25].

C. Effects of Zn doping

As pointed out for V-averievite [22], substitution of Cu²⁺ by nonmagnetic Zn²⁺ in the honeycomb layers is an interesting strategy to suppress the interlayer coupling and long-range magnetic order. We have performed this substitution for P-averievite, obtaining (CsCl)Cu₃Zn₂P₂O₁₀ (Zn-substituted P-averievite). Substitution of Zn ions in the honeycomb plane is energetically more favorable than substitution in the kagome layer due to the differing oxygen environments in

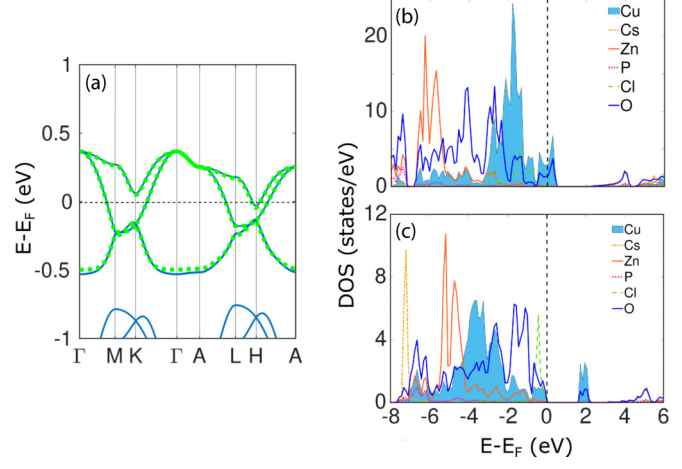


FIG. 5. DOS and band structure of Zn-substituted P-averievite. (a) Nonmagnetic GGA band structure (solid blue line) and the corresponding Wannier fitting to the three Cu $d_{x^2-y^2}$ bands (green dotted line). (b) Nonmagnetic GGA atom-projected DOS and (c) atom-projected DOS as obtained within GGA + U for an AFM spin configuration within kagome planes.

the two layers. In this situation, the kagome planes, separated by a large distance (8.45 Å), are the only magnetically active ones.

Figure 5 shows the corresponding GGA (nonmagnetic) and GGA + U (AFM) electronic structures of (CsCl)Cu₃Zn₂P₂O₁₀. In the nonmagnetic GGA band structure [Fig. 5(a)], there are three isolated bands around the Fermi level of only kagome Cu $d_{x^2-y^2}$ character due to the removal of the honeycomb coppers. There are clear Dirac crossings at the K and H points akin to the kagome single-orbital tight-binding model [39]. The same type of behavior has been reported in Zn-substituted V-averievite [22]. We have extracted tight-binding parameters for Zn-substituted averievite using MLWFs. To construct a basis of MLWFs in this case we use a narrow energy window of ~ 0.9 eV [see Fig. 5(a)] including only the Cu $d_{x^2-y^2}$ states. The corresponding fit [green dotted lines in Fig. 5(a)] matches well the band dispersion obtained from DFT calculations, indicating a faithful transformation to MLWFs. The spread of the derived Wannier functions is small ($\sim 1 \text{ Å}^2$).

The nearest-neighbor hopping integral is -123 meV, and the next-nearest-neighbor hopping integral is -28 meV. These values are comparable to those of the hopping integrals of Zn-substituted V-averievite [22]. The nonmagnetic GGA DOS [Fig. 5(b)] reveals that the Cu d bands crossing E_F hybridize strongly with O p states and that the valence bandwidth (\sim 8 eV) is reduced with respect to that of the parent compound. Zn²⁺ 3d states are completely filled and lie at lower energies.

The GGA + U DOS corresponding to the lowest-energy AFM spin configuration within kagome planes is depicted in Fig. 5(c). In the presence of U, the system is insulating with an estimated band gap of 1.7 eV, increased by 0.8 eV with respect to the parent compound. Like in P-averievite, the GGA + U DOS has main contributions from Cu d, O p, and Cl p states

right below E_F . Zn d states appear at lower energies. Unoccupied states are mostly Cu d in character, keeping a high degree of hybridization with O p states. The magnetic moments of Cu atoms in the kagome plane remain the same as in the parent material, $\sim 0.7 \mu_B$. The resulting exchange interactions for Zn-substituted averievite can be derived using the methodology described above. A dominant AFM $J_1 = 145$ K within the kagome plane is obtained from our calculations, 90 K lower than that for undoped P-averievite. A decrease in J_1 upon Zn substitution has also been reported in V-averievite [22], but the value of $J_1 \sim 170$ K is higher in that case. Experiments will have to be performed to confirm if substitution of Cu²⁺ by nonmagnetic Zn²⁺ can suppress long-range magnetic order in P-averievite as well.

IV. CONCLUSIONS

We have analyzed the effects of V by P substitution in the electronic and magnetic properties of the frustrated quantum magnet averievite. Both P- and V-averievite contain Cu²⁺ kagome layers sandwiched between Cu²⁺-P⁵⁺/Cu²⁺-V⁵⁺ honeycomb planes with pyrochlore slabs made of cornersharing Cu tetrahedra being formed. The tetrahedral geometry introduces magnetic frustration, as interactions within the Cu₄ units are AFM. Structural changes arise due to chemical pressure as the ionic radius of P⁵⁺ in tetrahedral coordination is over two times smaller than that of V⁵⁺. Our calculations reveal that the nearest-neighbor AFM coupling J_1 between kagome Cu atoms remains the same, ~235 K, in P- and V-averievite. In contrast, the interlayer AFM coupling J_2 between kagome and honeycomb Cu ions is 284 K in Paverievite, five times larger than the value of J_2 in its V counterpart. The stronger J_2 increases the degree of magnetic frustration within Cu tetrahedra in the phosphate material and is in agreement with the increase in the experimentally reported frustration index for P-averievite. Further, long-range magnetic order could be suppressed in Zn-substituted Paverievite, as the interlayer coupling is absent and the kagome spin- $\frac{1}{2}$ planes are the only magnetically active ones, making it a good candidate for QSL behavior.

As averievite is an oxide (vs traditional hydroxide platforms for spin- $\frac{1}{2}$ kagome physics), we anticipate this material should pose some advantages: (1) It should be less prone to disorder as Zn should substitute on the honeycomb copper sites based on crystal chemical considerations. (2) It shows a larger degree of p-d hybridization and should hence be more likely to promote metallicity (and possibly superconductivity). Based on these considerations, we hope our calculations stimulate further experiments in Zn-doped averievite and in other oxide spin- $\frac{1}{2}$ kagome systems.

ACKNOWLEDGMENTS

A.S.B. acknowledges NSF-DMR Grant No. 1904716. D.D. acknowledges ASU for startup funds. We acknowledge the ASU Research Computing Center for HPC resources.

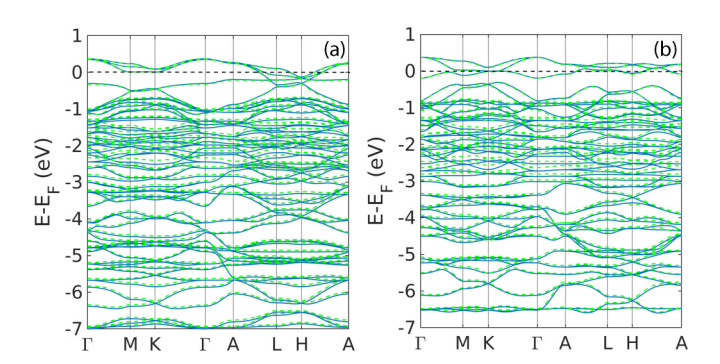


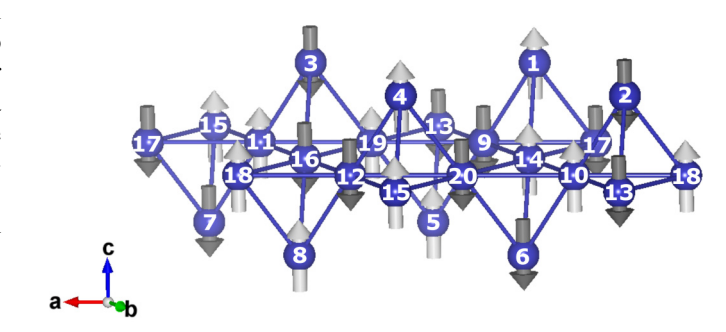
FIG. 6. Nonmagnetic GGA band structure (solid blue lines) and the corresponding Wannier fitting (green dotted lines) for (a) V-averievite and (b) P-averievite.

APPENDIX A: Wannier fitting of the DFT bands of undoped P- and V-averievite

A comparison between the band structures obtained from the GGA calculations and Wannier fitting for V- and P-averievite is shown in Fig 6.

APPENDIX B: Calculation of the exchange couplings

We have estimated magnetic exchange couplings up to next-nearest neighbors (NNNs), fitting the energy differences of different magnetic configurations to a Heisenberg model. Ten spin configurations were constructed in a 2 × 2 × 1 supercell with 20 Cu atoms: C1 (ground state), udduudduudduudduud (the labeling is defined in Fig. 7); C2, udduuddududddddddd; C3, ddduuddududdddduduud; C4, udduuddudddduudduud; C5, udduudduduuduuduud; C6, udduuddudddudduudduud; C7, udduudduduudduudduud; C8, udduuddududddduduud; C9, udduudduddddduduud; and C10, uuuuuuuuuuuuuuuu. The DFT energy differences ΔE between each of these configurations and the magnetic ground state (C1) are listed in Table III. Fitting the DFT energies (of five different spin configurations at a time) to a spin- $\frac{1}{2}$ Heisenberg model, we obtain, with small errors in the determination, the four exchange couplings J_{1-4} whose



C1. udduuddudduudduud

FIG. 7. C1 represents the magnetic ground state defined as udduudduduudduudduud, where $u \equiv \uparrow$ and $d \equiv \downarrow$ stand for majority and minority spins, respectively.

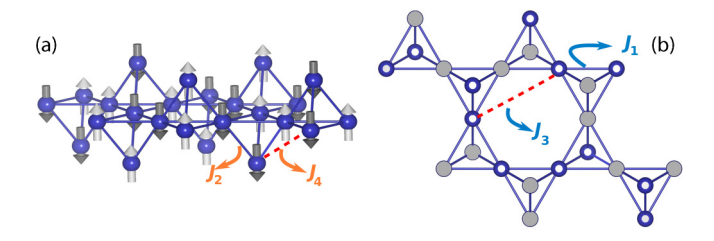


FIG. 8. Magnetic ground states for P- and V-averievite. Nearest-neighbor and next-nearest-neighbor (NNN) exchange paths are shown (a) between kagome and honeycomb Cu atoms (J_2 and J_4) and (b) between kagome Cu (J_1 and J_3). Red dashed lines represent the NNN exchange path.

paths are shown in Fig. 8. For P-averievite (V-averievite), J_1 (in-plane NN) is 234.9 (227.8) K, J_2 (out-of-plane NN) is 284.3 (51.7) K, J_3 (in-plane NNN) is -5.4 (-3.2) K, and J_4 (out-of-plane NNN) is 0.5 (1.7) K. It is evident from our

TABLE III. Energy difference per formula unit between different magnetic configurations with respect to the magnetic ground state (C1) defined by $\Delta E=0$.

$\Delta E \text{ (meV)/f.u.}$	$(CsCl)Cu_5P_2O_{10}\\$	$(CsCl)Cu_5V_2O_{10}$
C1	0.0	0.0
C2	15.2	14.8
C3	24.5	16.6
C4	12.2	2.1
C5	10.2	9.9
C6	6.1	1.1
C7	5.1	4.8
C8	15.3	15.1
C9	22.9	16.6
C10	111.1	63.4

calculations that J_1 and J_2 are the leading terms, whereas J_n for further exchange paths are significantly weaker.

- [1] P. Anderson, Mater. Res. Bull. 8, 153 (1973).
- [2] L. Balents, Nature (London) 464, 199 (2010).
- [3] M. R. Norman, Rev. Mod. Phys. 88, 041002 (2016).
- [4] L. Savary and L. Balents, Rep. Prog. Phys. 80, 016502 (2016).
- [5] Y. Zhou, K. Kanoda, and T.-K. Ng, Rev. Mod. Phys. 89, 025003 (2017).
- [6] M. J. Lawler, H.-Y. Kee, Y. B. Kim, and A. Vishwanath, Phys. Rev. Lett. 100, 227201 (2008).
- [7] I. I. Mazin, H. O. Jeschke, F. Lechermann, H. Lee, M. Fink, R. Thomale, and R. Valentí, Nat. Commun. 5, 4261 (2014).
- [8] T.-H. Han, J. S. Helton, S. Chu, D. G. Nocera, J. A. Rodriguez-Rivera, C. Broholm, and Y. S. Lee, Nature (London) 492, 406 (2012).
- [9] G. Baskaran, Z. Zou, and P. Anderson, Solid State Commun. 63, 973 (1987).
- [10] P. W. Anderson, Science 235, 1196 (1987).
- [11] J. S. Helton, K. Matan, M. P. Shores, E. A. Nytko, B. M. Bartlett, Y. Yoshida, Y. Takano, A. Suslov, Y. Qiu, J.-H. Chung, D. G. Nocera, and Y. S. Lee, Phys. Rev. Lett. 98, 107204 (2007).
- [12] M. P. Shores, E. A. Nytko, B. M. Bartlett, and D. G. Nocera, J. Am. Chem. Soc. 127, 13462 (2005).
- [13] R. H. Colman, A. Sinclair, and A. S. Wills, Chem. Mater. 23, 1811 (2011).
- [14] H. O. Jeschke, F. Salvat-Pujol, and R. Valentí, Phys. Rev. B 88, 075106 (2013).
- [15] Y. Iqbal, H. O. Jeschke, J. Reuther, R. Valentí, I. I. Mazin, M. Greiter, and R. Thomale, Phys. Rev. B 92, 220404(R) (2015).
- [16] S.-H. Lee, H. Kikuchi, Y. Qiu, B. Lake, Q. Huang, K. Habicht, and K. Kiefer, Nat. Mater. 6, 853 (2007).
- [17] M. A. de Vries, K. V. Kamenev, W. A. Kockelmann, J. Sanchez-Benitez, and A. Harrison, Phys. Rev. Lett. 100, 157205 (2008).
- [18] D. E. Freedman, T. H. Han, A. Prodi, P. Müller, Q.-Z. Huang, Y.-S. Chen, S. M. Webb, Y. S. Lee, T. M. McQueen, and D. G. Nocera, J. Am. Chem. Soc. 132, 16185 (2010).
- [19] Z. A. Kelly, M. J. Gallagher, and T. M. McQueen, Phys. Rev. X 6, 041007 (2016).

- [20] T.-H. Han, J. Singleton, and J. A. Schlueter, Phys. Rev. Lett. 113, 227203 (2014).
- [21] H. O. Jeschke, F. Salvat-Pujol, E. Gati, N. H. Hoang, B. Wolf, M. Lang, J. A. Schlueter, and R. Valentí, Phys. Rev. B 92, 094417 (2015).
- [22] A. S. Botana, H. Zheng, S. H. Lapidus, J. F. Mitchell, and M. R. Norman, Phys. Rev. B 98, 054421 (2018).
- [23] D. Boldrin, B. Fåk, M. Enderle, S. Bieri, J. Ollivier, S. Rols, P. Manuel, and A. S. Wills, Phys. Rev. B 91, 220408(R) (2015).
- [24] G. L. Starova, S. V. Krivovlchev, V. S. Fundamensky, and S. K. Filatov, Mineral. Mag. 61, 441 (1997).
- [25] M. J. Winiarski, T. T. Tran, J. R. Chamorro, and T. M. McQueen, Inorg. Chem. 58, 4328 (2019).
- [26] W. Kohn and L. J. Sham, Phys. Rev. 140, A1133 (1965).
- [27] P. Hohenberg and W. Kohn, Phys. Rev. 136, B864 (1964).
- [28] P. E. Blöchl, Phys. Rev. B 50, 17953 (1994).
- [29] G. Kresse and D. Joubert, Phys. Rev. B **59**, 1758 (1999).
- [30] G. Kresse and J. Furthmüller, Phys. Rev. B 54, 11169 (1996).
- [31] G. Kresse and J. Furthmüller, Comput. Mater. Sci. 6, 15 (1996).
- [32] J. P. Perdew, K. Burke, and M. Ernzerhof, Phys. Rev. Lett. 77, 3865 (1996).
- [33] S. L. Dudarev, G. A. Botton, S. Y. Savrasov, C. J. Humphreys, and A. P. Sutton, Phys. Rev. B 57, 1505 (1998).
- [34] J. Hubbard, Proc. R. Soc. London, Ser. A 276, 238 (1963).
- [35] A. A. Mostofi, J. R. Yates, G. Pizzi, Y.-S. Lee, I. Souza, D. Vanderbilt, and N. Marzari, Comput. Phys. Commun. 185, 2309 (2014).
- [36] A. P. Ramirez, Annu. Rev. Mater. Sci. 24, 453 (1994).
- [37] T. Arimori and H. Kawamura, J. Phys. Soc. Jpn. **70**, 3695 (2001).
- [38] X. Obradors, A. Labarta, A. Isalgué, J. Tejada, J. Rodriguez, and M. Pernet, Solid State Commun. 65, 189 (1988).
- [39] W.-S. Wang, Z.-Z. Li, Y.-Y. Xiang, and Q.-H. Wang, Phys. Rev. B **87**, 115135 (2013).